PMHS Lower Neck Load Calculation using Inverse Dynamics with Cervical Spine Kinematics and Neck Mass Properties

Yun-Seok Kang, Jason Stammen, Kevin Moorhouse, Rod Herriott, John H. Bolte IV

Abstract Most anthropomorphic test devices possess both an upper neck and a lower neck load cell to measure the risk of neck injury in crash simulations. For post-mortem human subject (PMHS) testing, the neck is frequently assumed to be a "massless link". It is unknown how much error is generated by this assumption. The objective of this study is to investigate lower neck loads using inverse dynamics techniques in frontal impacts. A mini-sled was designed to dynamically test a PMHS head-neck complex. A custom-sized elliptical ring was used for attaching upper thoracic structures in an anatomic configuration, to account for the contribution of these structures to the overall kinematics. A six-axis load cell was attached at the T3 level of the spine to measure the reaction loads at the upper thoracic spine. The PMHS head, C3, and C6 kinematics were measured to calculate lower neck loads using inverse dynamics techniques (IDT). A total of five PMHS tests were conducted to simulate a frontal impact. Lower neck loads were calculated using IDT, while considering either a massless link assumption (IDT-MLA) or the actual mass moment of inertia (MMI) and center of gravity (CG) of the neck, along with measured cervical kinematics (IDT-MMICG). The IDT-MMICG method resulted in less error from the measured forces and moments than the IDT-MLA method. It is recommended that instrumentation of at least one cervical level between C3 and C6 along with head/neck mass properties should be used for improved estimation of lower neck loads.

Keywords Cervical spine, lower neck loads, inverse dynamics, post-mortem human subjects

I. INTRODUCTION

Cervical spine injuries are common, and often costly, in motor vehicle crashes (MVC) [1-7]. Survivors with neck injuries in frontal and rear MVC often sustain injuries in the lower portion of the cervical spine [7]. With the exception of very young occupants (8 years or less), where the majority of neck injuries are in the OC/C1/C2 region [39], children and adults are more likely to sustain lower cervical spine and cervicothoracic junction injuries than upper cervical injuries [6]. In order to investigate neck injury tolerance and criteria, many studies have been conducted using human volunteers or post-mortem human surrogates (PMHS) in different impact directions [3-5][7-13]. Lower neck injuries have been commonly observed in experiments using PMHS in frontal, side and rear impacts [3-5][7-8][15]. The need exists to obtain accurate lower neck (cervicothoracic junction) biomechanical data, in order to develop an injury risk function for the lower neck in anthropomorphic test devices (ATDs). The addition of a lower neck criterion would improve the overall protection of the spine, neck and head in motor vehicle occupants [5][7][10].

Most ATDs possess both an upper and a lower neck load cell to measure the risk of neck injury in crash simulations. Upper neck criteria exist in Federal Motor Vehicle Safety Standard (FMVSS) No. 208, because upper neck injuries tend to be the most serious type of neck injury in frontal crashes [16]. Upper neck loads in PMHS testing are relatively easy to calculate using the inertial properties and kinematics of the head alone. However, addressing lower neck injuries, which occur more frequently than upper neck injuries in older children and adults, is more difficult. Accurate measurement of lower neck loads in PMHS that would allow for the creation of a lower neck injury risk function is a challenge due to the deformable properties of the neck. Frequently, the neck is considered a "massless link" for transferring upper neck loads to the T1 location of the spine [7][13][22][35-38]. However, the human neck does have mass and it typically exhibits significant nonlinear

Y. Kang, Ph.D. is a research scientist at Injury Biomechanics Research Center at the Ohio State University in Columbus, OH, USA (e-mail: yunseok.kang@osumc.edu, tel: 1.614.366.7584, fax: 1.614.292.7659). J. Stammen, Ph.D. and K. Moorhouse, Ph.D. are at National Highway Traffic Safety Administration (NHTSA), R. Herriott is at Transportation Research Center Inc. J. Bolte, Ph.D. is at the Ohio State University.

deformation (i.e. deformation of a whole neck) in a frontal impact event; thus error is expected from using this massless assumption.

With detailed deformation data and mass distribution characteristics of the PMHS neck, a more accurate assessment of lower neck loads may be possible. Kang *et al.* [4] introduced a new technique for obtaining detailed cervical spine kinematics information in PMHS undergoing rear-impact simulations. This technique can be used in a frontal configuration, as well to track the nonlinear deformation of the neck. Albery *et al*. [17] showed how mass distribution of the PMHS could be obtained by sectioning frozen PMHS and measuring the center of gravity (CG) location and mass moment of inertia (MMI) of each section. Together with calculation of the PMHS upper neck loads from the head mass properties and kinematics, these two techniques can be used to define PMHS lower neck response.

The main objective of this study is to combine detailed head/neck kinematics data with subject-specific head/neck mass properties in order to experimentally quantify the error in PMHS lower neck load calculation associated with the assumption that the neck can be treated as a massless link. With improved accuracy of lower neck loads, cervicothoracic spine injury criteria can be generated to monitor the risk of these injuries with ATDs. In addition, it would become more feasible to refine ATD spinal biofidelity by matching the ATD to PMHS cervicothoracic behavior.

II. METHODS

Post-mortem Human Subjects (PMHS)

The PMHS used for this study were available through Ohio State University's body donor program and all applicable NHTSA and university guidelines, as well as Institutional Review Board protocol, were reviewed and followed. Five unembalmed male PMHS (49 ± 16-year-old) were scanned using a computerized tomography (CT) and a fluoroscopic device (C-arm) to ensure there were no severely degenerated discs, osteophytes, or previous spinal surgery on the cervical and upper thoracic spine (Table I). In order to screen osteoporotic PMHS, the PMHS were scanned using Dual Energy X-ray Absorptiometry (DXA). Average subject height (177.6 ± 4.0 cm) was close to a 50th percentile male, while average subject weight (69.9 ± 4.3 kg) was lighter than the 50th percentile male. Anthropometric data from each PMHS head and neck is indicated in Table II.

TABLE I
PMHS INFORMATION

	Age	Cause of death	Lumbar BMD T-Score	Height (cm)	Weight (kg)
PMHS1	67	Pancreatic cancer	+1.1	184.5	71.0
PMHS2	57	Lung cancer	-2.0	175.0	64.0
PMHS3	54	Non-Small cell lung cancer	-1.9	175.3	74.1
PMHS4	25	Metastatic synovial sarcoma	-2.6	177.8	73.4
PMHS5	40	Metastatic melanoma	+0.4	175.3	67.0
Mean	**49**	**N/A**	**-1.0**	**177.6**	**69.9**
SD	**16**	**N/A**	**1.6**	**4.0**	**4.3**

TABLE II
PMHS HEAD AND NECK ANTHROPOMETRY (unit: cm)

	Head breadth	Head height	Head depth	Head circumference	Neck breadth	Neck depth	Neck circumference
PMHS1	15.5	23.5	19.0	56.4	11.7	10.6	36.5
PMHS2	14.1	22.0	19.0	58.0	12.7	9.2	35.5
PMHS3	15.3	23.0	20.3	61.0	12.7	12.8	43.0
PMHS4	13.5	20.9	18.8	57.0	11.5	8.8	35.5
PMHS5	13.9	23.6	19.0	57.6	11.4	13.5	41.5
Mean	**14.5**	**22.6**	**19.2**	**58.0**	**12.0**	**11.0**	**38.4**
SD	**0.9**	**1.1**	**0.6**	**1.8**	**0.6**	**2.1**	**3.6**

Test Set-up

A mini-sled was designed to dynamically test a PMHS head-neck complex (Fig. 1). Frontal impact tests were conducted on each PMHS at a nominal mini-sled velocity of 14 km/h with 5% of the coefficient of variation (Fig. A1, Appendix). A custom-sized elliptical ring (Fig. 1A) was used for attaching upper thoracic structures (1st rib, clavicles, muscles and skin) in an anatomic configuration, to account for the contribution of these structures to the overall kinematics of the head and neck. Detailed PMHS dissection information is provided in Appendix A. The ring was fixed to the mini-sled with turnbuckles (Fig. 1B) in line with six uniaxial load cells (Fig. 1C) that measure passive axial muscle forces during the event. The turnbuckles allowed for adjustment of initial tension in the neck muscles. Initial muscle tension was adjusted to 40–50 N, so that the total initial neck preload, including the head weight, was in the 75–100 N range, as specified in previous studies [18-19]. A six-axis load cell (Fig. 1D) was attached at the T3 level of the vertebral column to measure the reaction loads at the upper thoracic spine. The T3 vertebra was affixed within a custom cup (Fig. 1E) using Bondo® Body Filler (Bondo Corporation, Atlanta, GA, USA). The used Bondo and potting cup masses were measured and inertially compensated for in the measured T3 loads. The PMHS head was instrumented using six accelerometers and three angular rate sensors (ARS) installed on an external tetrahedron fixture (t6aω), shown in Fig. 1F. Three accelerometers and three ARS (3aω) were installed at both the C3 and C6 vertebra (see Kang *et al*. [4]) to capture kinematics of the upper and lower cervical spine (Fig. 1G) [4]. Each instrumentation mount was digitized using a FARO arm device (Faro Arm Technologies, Lake Mary, FL, USA) to transform data from the instrumentation to desired coordinate systems (e.g. body fixed local and sled or global coordinate systems). The PMHS head was supported by a harness that was attached to a head release system. The head release system was activated just prior to mini-sled motion.

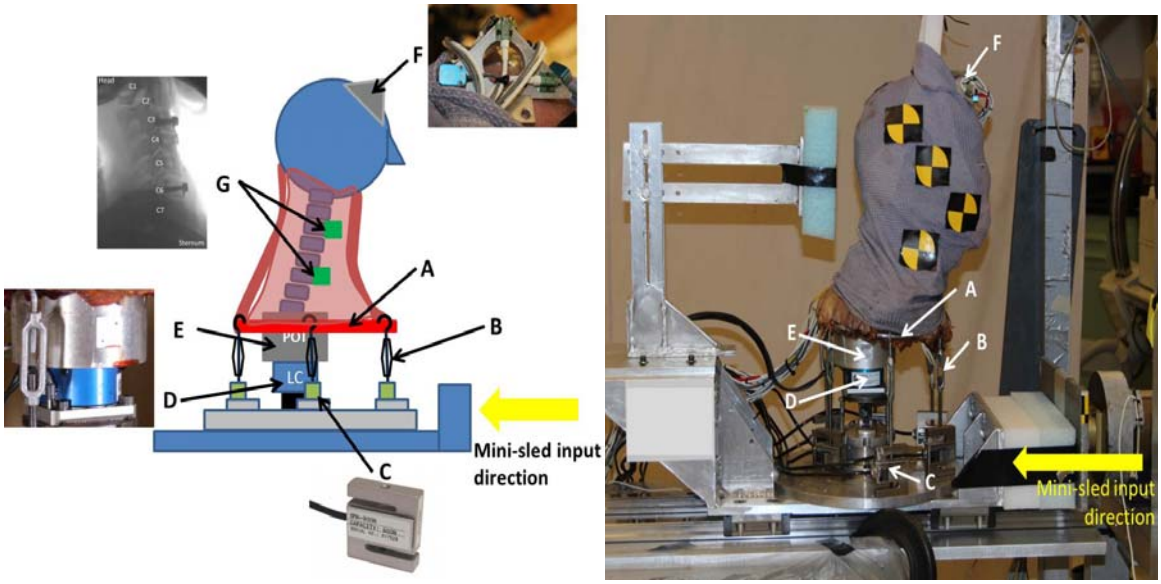

Fig. 1. Mini-sled set-up with PMHS head-neck complex.
A: Custom-sized elliptical ring.
B: Turnbuckles for initial muscle tension.
C: A custom potting cut for fixing T3 to the sled.
D: A six-axis load cell at T3.
E: A uniaxial load cell (6) for measuring muscle tension.
F: Head instrumentation (t6aω).
G: C3 and C6 instrumentation (3aω).

Mass properties of the head and neck

After the mini-sled tests, the head and neck were separated from one another and frozen, in order to measure the center of gravity (CG) and occipital condyle (OC) location, as well as the mass moment of inertia (MMI) of both the head and the neck. For the MMI measurement, an inverted pendulum device (Moment of Inertia Instrument Models XR – 50 and GB-3300AX, Space Electronics LLC, Berlin, CT) was used [20]. For the neck, the whole neck CG and MMI were determined first, then the neck was sectioned at the C4 level such that CG and MMI for upper (C1–C4) and lower (C4–C7) neck segments could be measured and used for calculating lower neck loads. CG and MMI information is presented in Tables AI and AII (Appendix A).

Data processing

The sampling frequency used in all testing was 20 kHz and all data obtained from the tests were filtered according to SAE J211. Data measured from the head instrumentation were transformed to the head CG in the body-fixed coordinate system, which was defined by digitizing the infraorbital notches and external auditory meati (x-axis forward and z-axis downward, according to SAE J211). The C3 and C6 data were transformed to the vertebral coordinate system (Fig. 2A, Appendix). Under the assumption that the PMHS head is a rigid body, a free body diagram (FBD) for upper neck (OC) loads is shown in Fig. 2 below. Upper neck forces were calculated using Equations 1 and 2, while upper neck moments were determined from Equations 3 and 4. Variables with underbars represent matrix forms that include x, y, and z components of the acceleration, velocity, position vector, forces and moments indicated in the Equations. In order to calculate kinematics and kinetics with respect to the global coordinate system, the transformation matrix (A) shown in Equation 5 was applied at each time step. ARS data were used to update the transformation matrix at each time increment. Time-dependent Euler angles (2-1-3 sequence) were used in the transformation matrix. Detailed information for obtaining the kinematics in body fixed local and global coordinate systems was provided in a previous study [21].

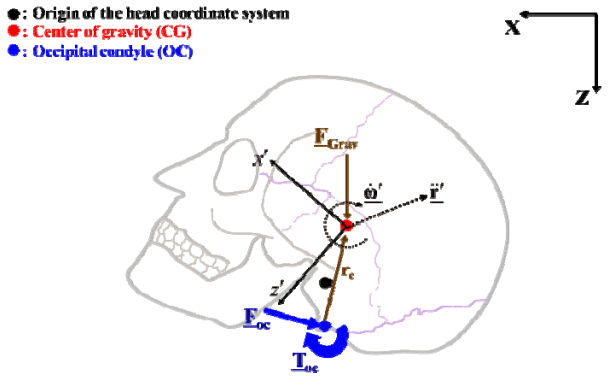

Fig. 2. Free body diagram of the PMHS head.

$$\underline{\mathbf{M}_{\mathbf{HD}}} \cdot \underline{\ddot{\mathbf{r}}'} = \underline{\mathbf{F}_{\mathbf{OC}}} + \underline{\mathbf{F}_{\mathbf{Grav}}} \quad (1)$$

$$\underline{\mathbf{F}_{\mathbf{OC}}} = \underline{\mathbf{M}_{\mathbf{HD}}} \cdot \underline{\ddot{\mathbf{r}}'} - \underline{\mathbf{F}_{\mathbf{Grav}}} \quad (2)$$

where: $\underline{\mathbf{M}_{\mathbf{HD}}} = \begin{bmatrix} m_{hd} & 0 & 0 \\ 0 & m_{hd} & 0 \\ 0 & 0 & m_{hd} \end{bmatrix}$ m_{hd}: head mass

$\underline{\ddot{\mathbf{r}}'} = [ax', ay', az']^T$ head CG linear acceleration in head coordinate system (x'-y'-z')

$\underline{\mathbf{F}_{\mathbf{OC}}} = [F_{OCx'}, F_{OCy'}, F_{OCz'}]^T$ forces at OC joint in head coordinate system

$\underline{\mathbf{F}_{\mathbf{Grav}}} = \underline{\mathbf{A}_{\mathbf{HD}}^{\mathbf{T}}} \cdot [0,0, m_{hd} \cdot g]^T$

where $\underline{\mathbf{A}_{\mathbf{HD}}}$ transformation matrix from the head coordinate system to the global frame

g: gravity (9.81 m/s^2)

$$\underline{\mathbf{J}'\dot{\boldsymbol{\omega}}'} + \underline{\tilde{\mathbf{r}}_{\mathbf{c}}} \cdot (\underline{\mathbf{M}_{\mathbf{HD}}} \cdot \underline{\ddot{\mathbf{r}}'}) = \underline{\mathbf{T}_{\mathbf{OC}}} - \underline{\tilde{\boldsymbol{\omega}}'} \cdot \underline{\mathbf{J}'} \cdot \underline{\boldsymbol{\omega}'} + \underline{\tilde{\mathbf{r}}_{\mathbf{c}}} \cdot \underline{\mathbf{F}_{\mathbf{Grav}}} \quad (3)$$

$$\underline{\mathbf{T}_{\mathbf{OC}}} = \underline{\mathbf{J}'\dot{\boldsymbol{\omega}}'} + \underline{\tilde{\mathbf{r}}_{\mathbf{c}}} \cdot (\underline{\mathbf{M}_{\mathbf{HD}}} \cdot \underline{\ddot{\mathbf{r}}'}) + \underline{\tilde{\boldsymbol{\omega}}'} \cdot \underline{\mathbf{J}'} \cdot \underline{\boldsymbol{\omega}'} - \underline{\tilde{\mathbf{r}}_{\mathbf{c}}} \cdot \underline{\mathbf{F}_{\mathbf{Grav}}} \quad (4)$$

where: $\underline{\mathbf{J}'} = \begin{bmatrix} J_{xx} & J_{xy} & J_{xz} \\ J_{yx} & J_{yy} & J_{yz} \\ J_{zx} & J_{zy} & J_{zz} \end{bmatrix}$ J is mass moment of inertia

$\underline{\dot{\boldsymbol{\omega}}'} = [\dot{\omega}_{x'}, \dot{\omega}_{y'}, \dot{\omega}_{z'}]^T$ angular acceleration in the head coordinate system

$\underline{\boldsymbol{\omega}'} = [\omega_{x'}, \omega_{y'}, \omega_{z'}]^T$ angular velocity in the head coordinate system

$\underline{\tilde{\mathbf{r}}_{\mathbf{c}}} = [r_{x'}, r_{y'}, r_{z'}]^T$ head CG position vector relative to the OC

$\underline{\mathbf{T_{OC}}} = [T_{OCx'}, T_{OCy'}, T_{OCz'}]^T$ moments at the OC in the head coordinate system

$$\underline{\mathbf{A}} = \begin{bmatrix} \cos\varphi\cos\sigma + \sin\varphi\sin\theta\sin\sigma & -\cos\varphi\sin\sigma + \sin\varphi\sin\theta\cos\sigma & \sin\varphi\cos\theta \\ \cos\theta\sin\sigma & \cos\theta\cos\sigma & -\sin\theta \\ -\sin\varphi\cos\sigma + \cos\varphi\sin\theta\sin\sigma & \sin\varphi\sin\sigma + \cos\varphi\sin\theta\cos\sigma & \cos\varphi\cos\theta \end{bmatrix} \quad (5)$$

where: φ - θ - σ are 2-1-3 sequence Euler angles

Inverse dynamics technique - massless link assumption (IDT-MLA) method

After upper neck loads were determined, the IDT-MLA method was applied to compute lower neck loads. Figure 3 shows the free body diagram for the IDT-MLA method. This method assumes that the neck is a massless link such that inertia of the neck can be ignored, as shown in Fig. 3. Lower neck loads were determined using Equations 6 and 7:

$$\underline{\mathbf{F_{LN}}} = \underline{\mathbf{A}_{\mathbf{LN}}^{\mathbf{T}}} \cdot \underline{\mathbf{A_{HD}}} \cdot \underline{\mathbf{F_{OC}}} \quad (6)$$

$$\underline{\mathbf{T_{LN}}} = \underline{\mathbf{A}_{\mathbf{LN}}^{\mathbf{T}}} \cdot \underline{\mathbf{A_{HD}}} \cdot (\underline{\mathbf{T_{OC}}} + \underline{\tilde{\mathbf{r}}_{\mathbf{OCLN}}} \cdot \underline{\mathbf{F_{OC}}}) \quad (7)$$

where: $\underline{\mathbf{F_{LN}}} = [F_{LNx'}, F_{LNy'}, F_{LNz'}]^T$ forces at lower neck with respect to lower neck coordinate system (x"-y"-z")

$\underline{\mathbf{A_{LN}}}$ transformation matrix from the lower neck coordinate system to the global frame

$\underline{\mathbf{A_{HD}}}$ transformation matrix from the head coordinate system to the global frame

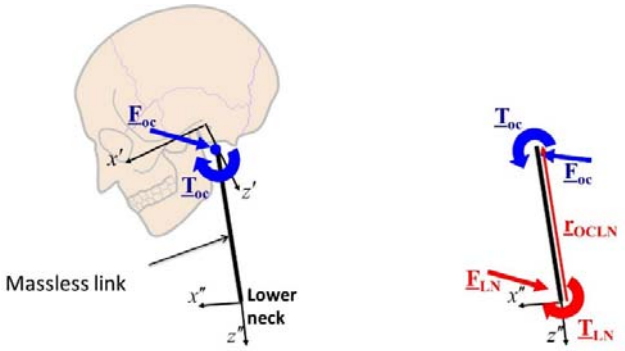

Fig. 3. Free body diagram for massless link assumption (IDT-MLA) method.

Inverse dynamics technique – mass moment of inertia and center of gravity (IDT-MMICG) method

First, the MMI and CG of the whole neck, upper neck segment and lower neck segment were determined using the inverse pendulum method [20], and then the IDT-MMICG method was employed to calculate lower neck loads. This method requires both inertial properties of the neck and cervical kinematics. Free Body Diagrams for both the whole neck (IDT-MMICG-WN) and the segmented neck (IDT-MMICG-SN) are provided in Fig. 4(a) and (b), respectively. This method was developed under the assumption that, while the IDT using the mass and inertial properties of the whole neck improves accuracy on the lower neck loads, the IDT considering a segmented neck (e.g. upper and lower cervical spine) can improve the accuracy even further since the

time-dependent change between the post-test static and dynamic CG location and MMI of both segments due to neck deformation would be expected to be smaller than when using the whole neck. For the FBD of the whole neck, shown in Fig. 4(a), lower neck loads were calculated by taking into account inertial forces and moments at the whole neck CG, gravitational force, and the OC loads (Equations 8–11). The only difference between IDT-MLA and IDT-MMICG is whether the initial forces are included in the equation (see Equation 6 vs. Equation 9). For the whole neck configuration (IDT-MMICG-WN), lower neck loads were calculated with respect to both C3 and C6 kinematics (hereafter referred to as the IDT-MMICG-WNC3 and IDT-MMICG-WNC6) as cervical kinematics were measured at both locations.

$$\underline{\mathbf{M}_{WN}}\,\underline{\ddot{\mathbf{r}}''_{WN}} = \underline{\mathbf{F}_{LN}} + \underline{\mathbf{A}_{LN}^{T}} \cdot \underline{\mathbf{F}_{Grav}} + \underline{\mathbf{A}_{LN}^{T}} \cdot \underline{\mathbf{A}_{HD}} \cdot \underline{\mathbf{F}_{OC}} \tag{8}$$

$$\underline{\mathbf{F}_{LN}} = \underline{\mathbf{M}_{WN}}\,\underline{\ddot{\mathbf{r}}''_{WN}} - \underline{\mathbf{A}_{LN}^{T}} \cdot \underline{\mathbf{F}_{Grav}} - \underline{\mathbf{A}_{LN}^{T}} \cdot \underline{\mathbf{A}_{HD}} \cdot \underline{\mathbf{F}_{OC}} \tag{9}$$

where: $\underline{\mathbf{M}_{WN}}$ = mass matrix of the whole neck

$\underline{\ddot{\mathbf{r}}''_{WN}}$ = linear acceleration at the whole neck CG with respect to orientation of lower neck coordinate system ($\underline{\mathbf{A}_{LN}^{T}}\ \underline{\ddot{\mathbf{r}}_{WN}}$)

where $\underline{\ddot{\mathbf{r}}_{WN}}$ is linear acceleration at the whole neck CG with respect to global coordinate system

$$\underline{\mathbf{J}''_{WN}} \cdot \underline{\dot{\boldsymbol{\omega}}''_{WN}} + \underline{\tilde{\mathbf{r}}_{CGLN}} \cdot (\underline{\mathbf{M}_{WN}} \cdot \underline{\ddot{\mathbf{r}}''_{WN}}) = \underline{\mathbf{T}_{LN}} - \underline{\tilde{\boldsymbol{\omega}}''_{WN}} \cdot \underline{\mathbf{J}''_{WN}} \cdot \underline{\boldsymbol{\omega}''_{WN}} + \underline{\mathbf{T}''_{Grav}} + \underline{\mathbf{T}''_{OC}} \tag{10}$$

$$\underline{\mathbf{T}_{LN}} = \underline{\mathbf{J}''_{WN}} \cdot \underline{\dot{\boldsymbol{\omega}}''_{WN}} + \underline{\tilde{\mathbf{r}}_{CGLN}} \cdot (\underline{\mathbf{M}_{WN}} \cdot \underline{\ddot{\mathbf{r}}''_{WN}}) + \underline{\tilde{\boldsymbol{\omega}}''_{WN}} \cdot \underline{\mathbf{J}''_{WN}} \cdot \underline{\boldsymbol{\omega}''_{WN}} - \underline{\mathbf{T}''_{Grav}} - \underline{\mathbf{T}''_{OC}} \tag{11}$$

where: $\underline{\mathbf{J}''_{WN}}$ = MMI of the whole cervical spine

$\underline{\dot{\boldsymbol{\omega}}''_{WN}}$ = angular acceleration with respect to lower neck coordinate system

$\underline{\boldsymbol{\omega}''_{WN}}$ = angular velocity with respect to lower neck coordinate system

$\underline{\mathbf{T}''_{Grav}} = \underline{\mathbf{A}_{LN}^{T}} \cdot \underline{\tilde{\mathbf{r}}_{CGLN}} \cdot \underline{\mathbf{F}_{Grav}}$

$\underline{\mathbf{T}''_{OC}} = \underline{\mathbf{A}_{LN}^{T}} \cdot \underline{\mathbf{A}_{HD}} \cdot (\underline{\mathbf{T}_{OC}} + \underline{\tilde{\mathbf{r}}_{OCLN}} \cdot \underline{\mathbf{F}_{OC}})$

$\underline{\tilde{\mathbf{r}}_{CGLN}}$ and $\underline{\tilde{\mathbf{r}}_{OCLN}}$ are CG and OC position vectors with respect to lower neck origin

For the segmented neck configuration shown in Fig. 4(b), lower neck loads can be computed using inertial properties of the upper and lower necks, C3 and C6 kinematics, gravitational force, and the OC loads. The equations can be expressed as:

$$\underline{\mathbf{M}_{UN}}\,\underline{\ddot{\mathbf{r}}''_{UN}} + \underline{\mathbf{M}_{LN}}\,\underline{\ddot{\mathbf{r}}''_{LN}} = \underline{\mathbf{F}_{LN}} + \underline{\mathbf{A}_{LN}^{T}} \cdot \underline{\mathbf{F}_{Grav}} + \underline{\mathbf{A}_{LN}^{T}} \cdot \underline{\mathbf{A}_{HD}} \cdot \underline{\mathbf{F}_{OC}} \tag{12}$$

$$\underline{\mathbf{F}_{LN}} = \underline{\mathbf{M}_{UN}}\,\underline{\ddot{\mathbf{r}}''_{UN}} + \underline{\mathbf{M}_{LN}}\,\underline{\ddot{\mathbf{r}}''_{LN}} - \underline{\mathbf{A}_{LN}^{T}} \cdot \underline{\mathbf{F}_{Grav}} - \underline{\mathbf{A}_{LN}^{T}} \cdot \underline{\mathbf{A}_{HD}} \cdot \underline{\mathbf{F}_{OC}} \tag{13}$$

where: $\underline{\mathbf{M}_{UN}}$ = mass matrix of the upper neck

$\underline{\mathbf{M}_{LN}}$ = mass matrix of the lower neck

$\underline{\ddot{\mathbf{r}}''_{UN}}$ = linear acceleration at the upper neck CG with respect to orientation of lower neck coordinate system ($\underline{\mathbf{A}_{LN}^{T}}\ \underline{\ddot{\mathbf{r}}_{UN}}$)

$\underline{\ddot{\mathbf{r}}''_{LN}}$ = linear acceleration at the lower neck CG with respect to orientation of lower neck coordinate system ($\underline{\mathbf{A}_{LN}^{T}}\ \underline{\ddot{\mathbf{r}}_{LN}}$)

where $\underline{\ddot{\mathbf{r}}_{UN}}$ and $\underline{\ddot{\mathbf{r}}_{LN}}$ are linear acceleration at the upper and lower neck CG with respect to global coordinate system, respectively

$$\begin{aligned}&\underline{\mathbf{J}''_{UN}} \cdot \underline{\dot{\boldsymbol{\omega}}''_{UN}} + \underline{\tilde{\mathbf{r}}_{UCLN}} \cdot (\underline{\mathbf{M}_{UN}} \cdot \underline{\ddot{\mathbf{r}}''_{UN}}) + \underline{\mathbf{J}''_{LN}} \cdot \underline{\dot{\boldsymbol{\omega}}''_{LN}} + \underline{\tilde{\mathbf{r}}_{LCLN}} \cdot (\underline{\mathbf{M}_{LN}} \cdot \underline{\ddot{\mathbf{r}}''_{LCS}}) \\ &= \underline{\mathbf{T}_{LN}} - \underline{\tilde{\boldsymbol{\omega}}''_{UN}} \cdot \underline{\mathbf{J}''_{UN}} \cdot \underline{\boldsymbol{\omega}''_{UN}} - \underline{\tilde{\boldsymbol{\omega}}''_{LN}} \cdot \underline{\mathbf{J}''_{LN}} \cdot \underline{\boldsymbol{\omega}''_{LN}} + \underline{\mathbf{T}''_{Grav}} + \underline{\mathbf{T}''_{OC}}\end{aligned} \tag{14}$$

$$\underline{\mathbf{T}}_{LN} = \underline{\mathbf{J}}''_{UN} \cdot \underline{\dot{\boldsymbol{\omega}}}''_{UN} + \underline{\tilde{\mathbf{r}}}_{UCLN} \cdot (\underline{\mathbf{M}}_{UN} \cdot \underline{\ddot{\mathbf{r}}}''_{UN}) + \underline{\mathbf{J}}''_{LN} \cdot \underline{\dot{\boldsymbol{\omega}}}''_{LN} + \underline{\tilde{\mathbf{r}}}_{LCLN} \cdot (\underline{\mathbf{M}}_{LN} \cdot \underline{\ddot{\mathbf{r}}}''_{LN}) + \underline{\tilde{\boldsymbol{\omega}}}''_{UN} \cdot \underline{\mathbf{J}}''_{UN} \cdot \underline{\boldsymbol{\omega}}''_{UN} + \underline{\tilde{\boldsymbol{\omega}}}''_{LN} \cdot \underline{\mathbf{J}}''_{LN} \cdot \underline{\boldsymbol{\omega}}''_{LN} - \underline{\mathbf{T}}''_{Grav} - \underline{\mathbf{T}}''_{OC} \quad (15)$$

where: $\underline{\mathbf{J}}''_{UN}$ and $\underline{\mathbf{J}}''_{LN}$ = MMI of the upper and lower neck

$\underline{\dot{\boldsymbol{\omega}}}''_{UN}$ and $\underline{\dot{\boldsymbol{\omega}}}''_{LN}$ = angular acceleration of the upper and lower neck in lower neck coordinate system

$\underline{\boldsymbol{\omega}}''_{UN}$ and $\underline{\boldsymbol{\omega}}''_{LN}$ = angular velocity of the upper and lower neck in lower neck coordinate system

$\underline{\tilde{\mathbf{r}}}_{UCLN}$ and $\underline{\tilde{\mathbf{r}}}_{LCLN}$ = upper and lower neck CG position vector relative to lower neck origin

(a) Whole neck. (b) Upper and lower neck.

Fig. 4. Free body diagram for MMI and CG method.

Since T3 vertebra load and muscle passive axial load were measured separately but both contribute to the overall neck response, these two loads were combined to be used as the baseline (target) measured forces and moments, such as the force in the Z direction and moment in the Y direction, shown in Fig. 5. Target measured forces in the X and Z axes and moment in the Y axis can be expressed as Equations 16, 17 and 18, respectively. These target loads were compared to those computed from IDT-MLA and IDT-MMICG methods.

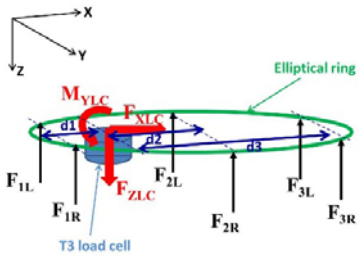

Fig. 5. Free body diagram of the T3 load cell and muscle tension load cells.

$$F_{Xtar} = F_{XLC} \quad (16)$$

$$F_{Ztar} = F_{ZLC} - (F_{1L} + F_{1R} + F_{21L} + F_{2R} + F_{3L} + F_{3R}) \quad (17)$$

$$M_{Ytar} = M_{YLC} - d1 \times (F_{1L} + F_{1R}) + d2 \times (F_{2L} + F_{2R}) + d3 \times (F_{3L} + F_{3R}) \quad (18)$$

where: $F_{Xtar}, F_{Ztar}, and\ M_{Ytar}$ are target forces and moments used for assessing IDT-MLA and IDT-MMICG methods.

In order to quantitatively assess the accuracy of the calculations using the various IDT methods with respect to the target measurement, both the peak differences and the normalized root mean squared deviation (NRMSD) were calculated, as shown in Equations 19 and 20:

$$\%\,Peak\ diff = \frac{|\text{peak target} - \text{peak IDT}|}{0.5 * |\text{peak target} + \text{peak IDT}|} \times 100 \quad (19)$$

$$NRMSD = \frac{\sqrt{\frac{1}{n}\sum_{i=0}^{n}(Y_i - Y_i')^2}}{Y'_{\max} - Y'_{\min}} \quad (20)$$

where: *n* is the total number of data points*, Y'max* and *Y'min* represent the maximum and minimum values of the target data*, Yi* and *Y'i* are the ith data point obtained from the response being evaluated (e.g. IDT data) and the ith data point obtained from the response being compared to (target forces and moments), respectively.

Percent peak differences and NRMSD were evaluated by comparing the target measured loads to lower neck loads determined from IDT-MLA, IDT-MMICG-WNC3, IDT-MMICG-WNC6, and IDT-MMICG-SN.

III. RESULTS

The target measured lower neck loads and those calculated from IDT methods are found in Fig. 6. Qualitatively, IDT-MMICG methods (i.e. both IDT-MMICG_WN and SN) exhibited better agreement with the target loads (lower neck Fx, Fz and My) than those from IDT-MLA that were obtained in the five PMHS tests. It is notable that IDT-MLA results were always lower in magnitude than the target loads, and this trend was consistent across all five PMHS tests. Average percent peak differences and NRMSD from the five PMHS tests are shown in Figs 7 and 8, respectively. The results from percent peak difference analysis (Fig. 7) show that the peak Fx and peak My were not improved by using the IDT-MMICG method, while the peak Fz determined from IDT-MMICG exhibited lower percent peak differences than those determined from IDT-MLA. The opposite was true in NRMSD analysis (Fig. 8). The NRMSD for Fx and My determined from IDT-MMICG were less than those from the IDT-MLA, while NRMSD values calculated from Fz were similar between IDT-MLA and IDT-MMICG. These results show that the massless link assumption would yield, at minimum, a 16% under-prediction of peak values (average 24% in Fx, 16% in Fz, and 21% in My), shown in Fig 7. In addition, the massless assumption yielded a NRMSD over 20% for both Fx (24%) and My (28%) and less than 10% for Fz (8%), as shown in Fig 8. Curves resulting from IDT-MMICG had shapes/phases qualitatively closer to the target time-histories than those from IDT-MLA (Fig. 6). The improvement provided by the segmented neck approach (IDT-MMIGC-SN) was minimal when compared to IDT-MMICG-WNC3 and IDT-MMICG-WNC6 (Figs 7 and 8).

IV. DISCUSSION

This study investigated the accuracy of various inverse dynamics techniques for calculating lower neck loads. The PMHS neck has traditionally been assumed to be a massless link for lower neck load calculation [7][13], but in reality the neck is a deformable body with mass. In order to evaluate and improve upon ATD response, accurate measurement of lower neck loads is necessary [22]. IDT works well when rigid body components are considered, such as when three-dimensional dynamics of ATD heads are used to accurately calculate upper neck forces [23]. However, the human body is not composed of rigid bodies with kinematic joints, so the use of IDT for determining loads on PMHS typically produces inevitable error when kinetics are estimated in a flexible part of the body, such as the neck. The present study attempted to quantify and reduce this error by including accurately measured inertial properties and cervical kinematics.

Accuracy of upper neck load calculation directly affects the lower neck loads, as shown in Eqs. 8-15. In scenarios without head contact, head kinematics and inertial properties (e.g. mass, MMI, CG and OC) are required to calculate upper neck loads. The upper neck moments from IDT are highly dependent on head angular acceleration measurement. Moreover, the angular acceleration and angular velocity also influences accuracy of the transformed linear acceleration to the CG of the head, because those are required to transform data from the externally located head instrumentation to the center of gravity of the PMHS head. Therefore, the angular acceleration and angular velocity can also influence accuracy of the upper neck forces. In order to measure accurate angular kinematics of the head, various head instrumentation techniques and schemes have been developed and validated extensively [21][24-27]. In this study, the t6aω technique proposed by Kang *et al*. [25] was used because this method provides very accurate measurement of head angular kinematics for two primary reasons: angular acceleration is determined using simple algebraic equations; and angular velocity is

directly measured from the ARS [21][25].

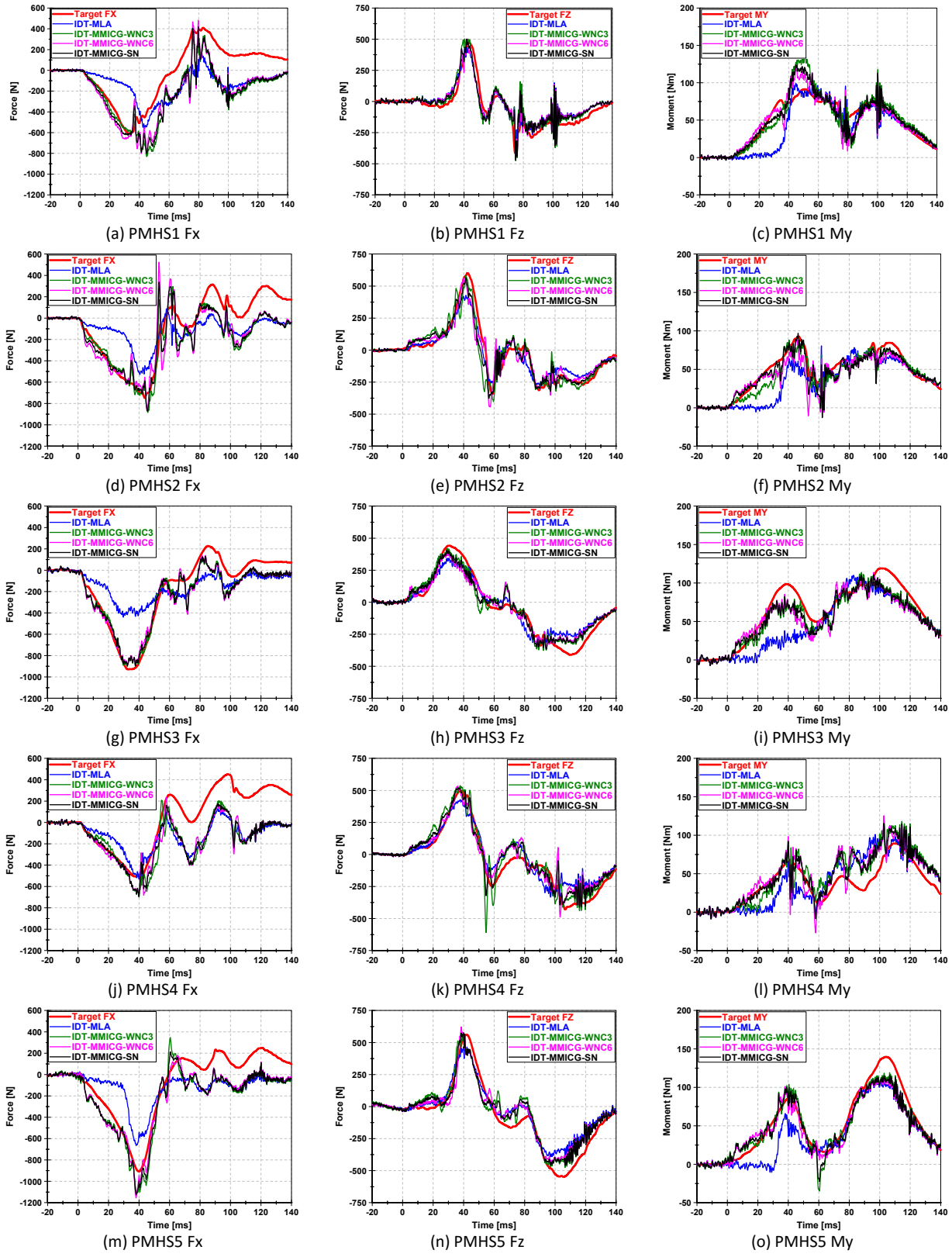

(a) PMHS1 Fx (b) PMHS1 Fz (c) PMHS1 My

(d) PMHS2 Fx (e) PMHS2 Fz (f) PMHS2 My

(g) PMHS3 Fx (h) PMHS3 Fz (i) PMHS3 My

(j) PMHS4 Fx (k) PMHS4 Fz (l) PMHS4 My

(m) PMHS5 Fx (n) PMHS5 Fz (o) PMHS5 My

Fig. 6. Target loads vs. IDT methods.

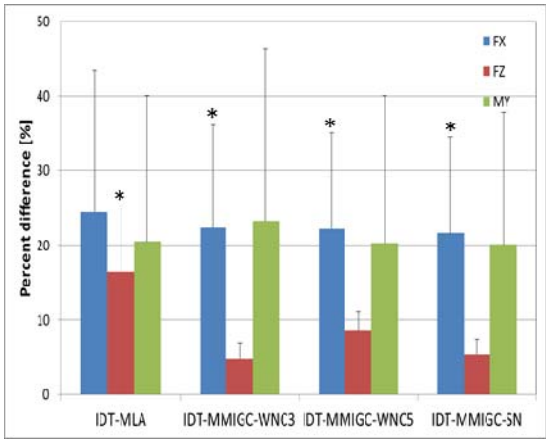

Fig. 7. Average percent peak differences for all five PMHS.
*: p-value < 0.05 from t-test (target vs. IDT methods)

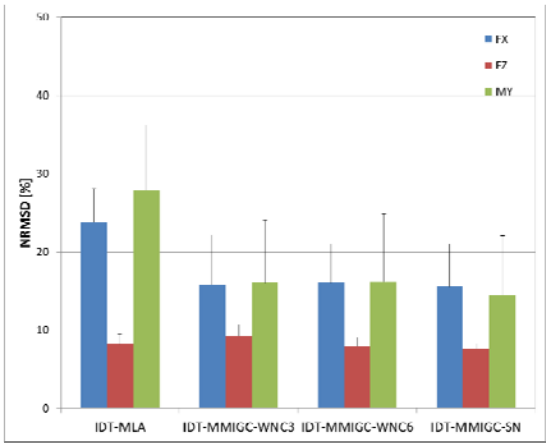

Fig. 8. Average NRMSD for all five PMHS.

The measurement of PMHS head inertial properties (mass, MMI, CG and OC locations) is also critical for accurately calculating upper neck loads. Inertial properties of the head and neck have been characterized previously using PMHS and human volunteers [28-34], and it has been demonstrated how error in inertial properties can produce inaccurate upper neck loads. Pintar *et al*. [9] found that 3 mm CG location differences can affect upper neck loads by as much as 17%, and 5% of error in MMI can result in 17% error in upper neck moments. In order to have accurate and repeatable measurements on inertial properties of the head and neck, this study used a reliable device validated by Self *et al*. [20].

The IDT-MLA method has been used historically for estimating lower neck forces in PMHS studies in both frontal and rear impacts [7][13]. This massless link method can possibly be used with minimal error when cervical kinematics are small enough to be ignored (e.g. lower severity volunteer testing). Based on the results from this current study, the lower neck loads from IDT-MLA can be under-estimated by over 20%. It is likely that this under-estimation is greater in even higher severity test conditions. In this study, IDT-MMICG methods using both whole necks and segmented necks were investigated to better understand the value of including the mass properties of the neck in the calculation of lower neck loads. IDT-MMICG improved the accuracy of Fz, while IDT-MMICG-SN did not exhibit a significant improvement over IDT-MMICG-WN. There was no difference using the two segments over the whole neck because C3 and C6 neck kinematics with respect to the lower neck coordinate system were quite similar. In effect, the MMI/CG had reached their capacity in improving accuracy because of the neck's viscoelastic characteristics causing time-dependent changes in mass distribution during the event. Fx and My calculated with IDT-MMICG had similar error in the peak values as compared to error with IDT-MLA. Time-history evaluation (i.e. NRMSD) between IDT-MMICG-calculated loads and the target measured loads also showed improvement from IDT-MLA. In order to use IDT-MMICG methods, the neck had to be regarded as a rigid body. However, the neck exhibited nonlinear deformation during the event; therefore, the neck segment CG location and MMI both changed over time. For this reason, IDT-MMICG still produces error from the target lower neck measurements. However, the shapes and phases of all the responses, as well as the peak Fz, were closer to the target loads by taking into account the inertial properties and cervical kinematics of the neck in the inverse dynamics equations. Given these results, it is recommended that, when possible, at least one cervical level between C3 and C6 be instrumented and the PMHS head and neck mass properties be measured post-test for improved estimation of lower neck loads.

Limitations

This study only considered a non-head-contacting condition. If there are external loads applied to the head (e.g. head contacting interior structures in a vehicle), determining accurate upper neck loads is a challenge as external loads have to be measured accurately and in three dimensions. In this case, calculating lower neck loads is more complicated and most likely to be compromised due to errors in measuring the external source. For this reason, frontal impact mini-sled tests without head contact were used in this study to compare IDT methods.

In order to use IDT, the head and neck had to be treated as rigid bodies in this study. However, the human neck is actually composed of deformable components, resulting in changes in CG locations and MMI during events. Measuring accurate time-dependent CG and MMI would likely improve the accuracy of the lower neck load calculations; however, tracking within-structure changes in mass distribution over time in an experiment such as this is extremely difficult. Additionally, only inertia terms were considered in the IDT-MMICG methods investigated in this study. Viscoelastic properties of the neck were not considered; that is, there were no stiffness and damping terms in the inverse dynamics equations used in this study. Future analysis should be performed to determine stiffness and damping coefficients of the neck by using optimization techniques.

V. CONCLUSIONS

This study investigated various methods for calculating lower neck loads using inverse dynamics techniques. A mini-sled was designed to dynamically test a PMHS head-neck complex. A custom-sized elliptical ring was used for attaching upper thoracic structures in an anatomic configuration, to account for the contribution of these structures to the overall kinematics. A total of five PMHS tests were conducted in a frontal impact mini-sled configuration. IDT-MMICG methods that included detailed cervical spine kinematics and neck mass properties provided a more accurate calculation of axial lower neck force (Fz) than using the massless link assumption (IDT-MLA). IDT-MMICG also resulted in qualitatively closer shapes and phases in the overall force and moment time histories than IDT-MLA. Results from the IDT-MLA method underestimated the target measurement by 16% or more. This amount of error should be considered when the IDT-MLA method is used in PMHS tests. Instrumentation of at least one cervical level between C3 and C6 along with head/neck mass properties should be used for improved estimation of lower neck loads.

VI. ACKNOWLEDGEMENTS

The authors would like to thank Allison Yard, Arriana Willis, David Stark, Michelle Murach, Sam Goldman and all IBRC members of the Ohio State University, and Brian Suntay from Transportation Research Center, Inc. for their considerable support during testing days.

VII. REFERENCES

[1] Quinlan, K. P., Annest, J. L., Myers, B., Ryan, G., Hill, H. (2004) Neck strains and sprains among motor vehicle occupants—United States, 2000. *Accident Analysis & Prevention*, **36**(1): pp.21–7.

[2] Kullgren, A., Krafft, M., Ydenius, A., Lie, A., Tingvall, C. Developments in car safety with respect to disability: injury distributions for car occupants in cars from the 80's and 90's. *Proceedings of International IRCOBI Conference,* 2002, Munich, Germany.

[3] Kang, Y. S., Bolte IV, J. H. *et al*. (2012) Biomechanical responses of PMHS in moderate-speed rear impacts and development of response targets for evaluating the internal and external biofidelity of ATDs. *Stapp car crash journal*, **56**: p.105.

[4] Kang, Y. S., Moorhouse, K., Herriott, R., Bolte IV, J. H. (2013) Comparison of cervical vertebrae rotations for PMHS and BioRID II in rear impacts. *Traffic injury prevention*, **14**(sup1): pp.S136–47.

[5] McIntosh, A. S., Kallieris, D., Frechede, B. (2007) Neck injury tolerance under inertial loads in side impacts. *Accident Analysis & Prevention,* **39**(2): pp.326–33.

[6] Goldberg, W., Mueller, C. *et al*. NEXUS Group. (2001) Distribution and patterns of blunt traumatic cervical spine injury. *Annals of emergency medicine,* **31;38**(1): pp.17–21.

[7] Pintar, F. A., Yoganandan, N., Maiman, D. J. (2010) Lower cervical spine loading in frontal sled tests using inverse dynamics: potential applications for lower neck injury criteria. *Stapp Car Crash Journal*, **54**: p.133.

[8] Kallieris, D., Mattern, R., Miltner, E., Schmidt, G., Stein, K. (1991) Considerations for a neck injury criterion. *SAE Technical paper*.

[9] Pintar, F. A., Yoganandan, N., Baisden, J. (2005) Characterizing occipital condyle loads under high-speed head rotation. *Stapp Car Crash Journal,* **49**: p.33.

[10] Pintar, F. A., Voo, L. M., Yoganandan, N. A., Cho, T. H., Maiman, D. J. Mechanisms of hyperflexion cervical spine injury. *Proceedings of IRCOBI Conference,* 1998, Göteberg, Sweden.

[11] Panjabi, M. M., Pearson, A. M. *et al*. (2004) Cervical spine ligament injury during simulated frontal impact. *Spine.* **29**(21): pp.2395–403.

[12] Pearson, A. M., Panjabi, M. M. *et al*. (2005) Frontal impact causes ligamentous cervical spine injury. *Spine*, **30**(16): pp.1852–8.

[13] Sundararajan, S., Prasad, P. *et al*. (2004) Effect of head-neck position on cervical facet stretch of post mortem human subjects during low speed rear end impacts. *Stapp Car Crash J.,* **48**: pp.331–72.

[14] Prasad, P., Kim, A., Weerappuli, D. P. Biofidelity of anthropomorphic test devices for rear impact. *Proceedings of Stapp Car Crash Conference,* 1997 (Vol. 41, pp.387–415). Society of Automotive Engineers, SAE.

[15] Yoganandan, N., Pintar, F. A. *et al*. (2000) Biomechanics of human occupants in simulated rear crashes: documentation of neck injuries and comparison of injury criteria. *Stapp car crash journal*, **44**: pp.189–204.

[16] NHTSA. (2000) FMVSS 208 Occupant Crash Protection. Docket of Federal Regulations 49, Part 571.208, US Government Printing Office, Washington, D.C.

[17] Albery, C. B., Whitestone, J. J., A Comparison of Cadaveric Human Head Masses, Centers of Gravity and Moments of Inertia: Direct Measurement vs. Computed Tomographic Calculation. *Proceedings of the Aerospace Medical Association (AsMA) Annual Scientific Meeting*, 2003, San Antonio, Texas.

[18] Miura, T., Panjabi, M. M., Cripton, P. A. (2002) A method to simulate in vivo cervical spine kinematics using in vitro compressive preload. *Spine*, **27**(1): pp.43–8.

[19] Nelson, T. S., Cripton, P. A. (2010) A new biofidelic sagittal plane surrogate neck for head-first impacts. *Traffic injury prevention,* **11**(3): pp.309–19.

[20] Self, B. P., Spittle, E. K., Kaleps, L. and Albery, C. B. (1992) Accuracy and repeatability of the standard automated mass properties measurement system. AL-TR-1992-0137, Armstrong Laboratory. *Wright-Patterson AFB*, Ohio.

[21] Kang, Y. S., Moorhouse, K., Bolte, J. H. (2011) Measurement of six degrees of freedom head kinematics in impact conditions employing six accelerometers and three angular rate sensors (6aω configuration). *Journal of biomechanical engineering*, **133**(11).

[22] Yoganandan, N., Pintar, F. A. *et al*. Upper and lower neck loads in belted human surrogates in frontal impacts. *Proceedings of Annals of Advances in Automotive Medicine/Annual Scientific Conference,* 2012 (Vol. 56, p.125), Seattle, Washington.

[23] Viano, D. C., Melvin, J. W. *et al*. (1986) Measurement of head dynamics and facial contact forces in the Hybrid III dummy. *SAE Technical Paper*.

[24] Yoganandan, N., Zhang, J., Pintar, F. A., Liu, Y. K. (2006) Lightweight low-profile nine-accelerometer package to obtain head angular accelerations in short-duration impacts. *Journal of Biomechanics*, **39**(7): pp.1347–54.

[25] Kang, Y. S., Moorhouse, K., Bolte IV, J. H. Instrumentation Technique for Measuring Six Degrees of Freedom Head Kinematics in Impact Conditions using Six-Accelerometers and Three-Angular Rate Sensors (6aω Configuration) on a Lightweight Tetrahedron Fixture. *Proceedings of 24th International Technical Conference on the Enhanced Safety of Vehicles (ESV),* 2015 (No. 15-0288), Gothenburg, Sweden.

[26] Padgaonkar, A. J., Krieger, K. W., King, A. I. (1975) Measurement of angular acceleration of a rigid body using linear accelerometers. *Journal of Applied Mechanics*, **42**(3): pp.552–6.

[27] Martin, P. G., Hall, G. W., Crandall, J. R., Pilkey, W. D. (1998) Measuring the acceleration of a rigid body. Shock and *Vibration*, **5**(4): pp.211–24.

[28] Clauser, C. E., McConvile, J. T. and Young, J. W. (1969) Weight, volume, and center of mass of segments of the human body, AMRL-TR-69-70. *Wright-Patterson AFB*, Ohio.

[29] Becker, E. B. Measurement of mass distribution parameters of anatomical segments. *Proceedings of 16th STAPP Car Crash Conference,* 1972, Detroit, Michigan.

[30] Walker, L. B., Harris, E. H.,Pontius, U. Mass, volume, center of mass, and mass moment of inertia of head and neck of human body. *Proceedings of STAPP Car Crash Conference*, 1973, pp.525–38, Oklahoma City, Oklahoma.

[31] Chandler, R. F., Clauser, C. E., McConville, J. T., Reynolds, H. M. and Young, J. W. (1974) Investigation of inertial properties of the human body, AMRL-TR-74-137. *Wright-Patterson AFB*, Ohio.

[32] Beier, G., Schuller, E. *et al*. Center of gravity and moments of inertia of human heads. *Proceedings of International IRCOBI Conference,* 1980, Birmingham, UK.

[33] McConville, J. T., Churchill, T. D., Kaleps, I., Clauser, C. E. and Cuzzi, J. (1980) Anthropometric relationships of body and body segment moment of inertia. AFAMRL-TR-80-119. *Wright-Patterson AFB*, Ohio, 190.

[34] Kaleps, I., Clauser, C. E. *et al*. (1984) Investigation into mass distribution properties of the human body and its segments. *Ergonomics*, **27**(12): pp.1225–37.

[35] Philippens, M.M.G.M., Wismans, J., Forbes, P.A., Yoganandan, N., Pintar, F.A. and Soltis, S.J., (2009) ES2 neck injury assessment reference values for lateral loading in side facing seats. Stapp car crash journal, **53**, p.421.

[36] Wismans, J., Philippens, M., Van Oorschot, E., Kallieris, D. and Mattern, R., Comparison of human volunteer and cadaver head-neck response in frontal flexion *Proceedings of STAPP Car Crash Conference*, 1987, New Orleans, Louisiana.

[37] Wismans, J., Spenny, C. H. Head-neck response in frontal flexion. *Proceedings of STAPP Car Crash Conference*, 1984 (Vol. 28, pp. 161-171), Chicago, Illinois.

[38] Yoganandan, N.A., Pintar, F.A., Moore, J., Schlick, M., Humm, J., Rinaldi, J. and Maiman, D.J. Sled tests using the THOR-NT device and post mortem human surrogates in frontal impacts. *Proceedings of IRCOBI Conference*, 2012, Dublin, Ireland.

[39] Platzer, P., Jaindl, M., Thalhammer, G., Dittrich, S., Kutscha-Lissberg, F., Vecsei, V., Gaebler, C. Cervical spine injuries in pediatric patients. Journal of Trauma and Acute Care Surgery. 2007 Feb 1;**62**(2):389-96.

VIII. APPENDIX

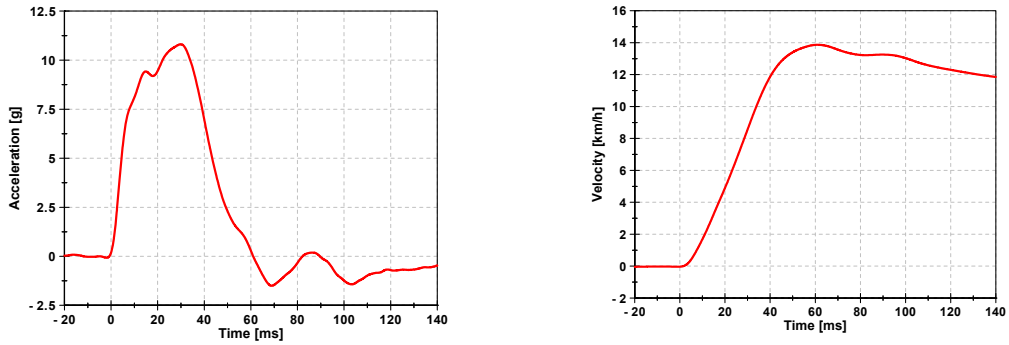

(a) acceleration (b) velocity

Fig. A1. Mini-sled inputs.

Procedure for dissection

1. Posterior dissection
    a. Cut trapezius muscle along the spine of the scapula.
    b. Cut levator scapulae muscle and rhomboid major and minor muscles along the scapula so that the scapula will hang loose.
    c. Make an incision and cut from the spine of the scapula to T3 (going through the deep muscles of the back, including the erector spinae muscles).
    d. Cut along spinous processes, starting with T3 and running superior to remove the spinal ligaments.
    e. Peel back all muscle (as a whole and towards the head) gradually to expose and cut ribs 2 and 3.
2. Anterior dissection
    a. Remove the skin below the clavicle to expose the bone and cut through acromioclavicular joint and coracoclavicular ligaments.
    b. Make an incision from the clavicle around the front of the thorax to sternum.
    c. Peel back all muscle toward the head.
    d. Cut the sternum at the sternal angle above rib 2.
    e. Follow the cut made at the sternal angle along rib 2, cutting through tissue down to the lungs and thoracic cavity.
    f. Cut through the disc and facet joints between T3 and T4 (anterior and posterior longitudinal ligaments, ligamentum flavum, and spinal ligament need to be cut).

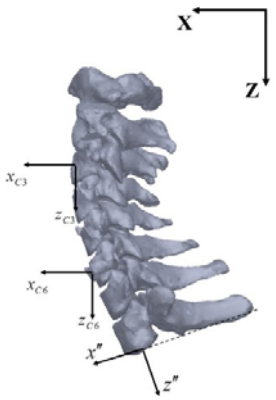

Fig. A2. C3, C6 and lower neck coordinate system: for IDT methods, C3 and C6 coordinate system was rotated to lower neck coordinate system such that C3 and C6 kinematics can be determined with respect to the lower neck coordinate system.

Head and neck inertial properties

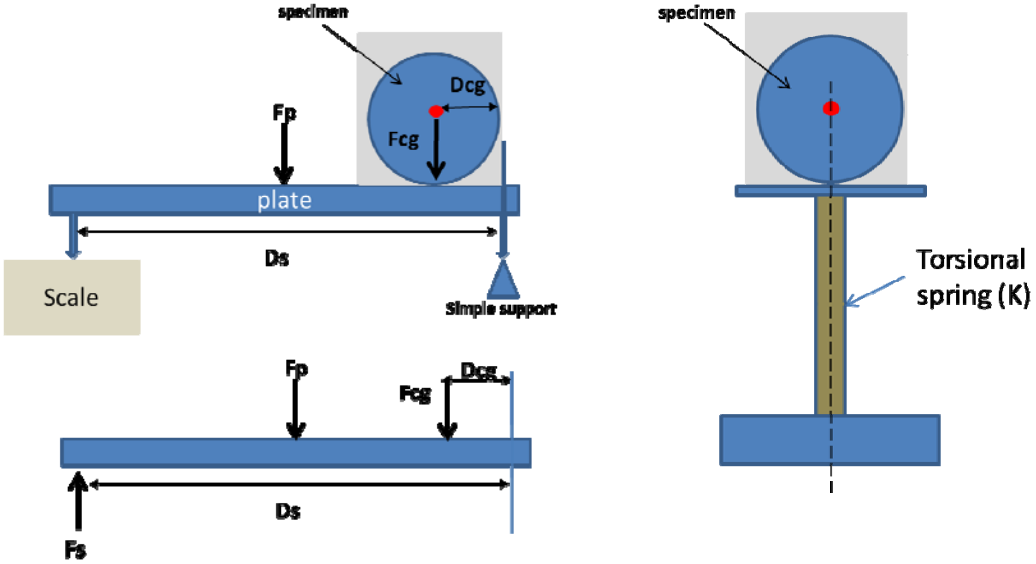

(a) CG measurement (b) MMI measurement

Fig. A2. Simplified diagram for measuring inertial properties

$$\sum \mathbf{M} = \mathbf{0} : \mathbf{Fs} \cdot \mathbf{Ds} - \mathbf{Fp} \cdot \frac{\mathbf{Ds}}{\mathbf{2}} - \mathbf{Fcg} \cdot \mathbf{Dcg} = \mathbf{0} \quad \text{(A1)}$$

$$\mathbf{Dcg} = \frac{(\mathbf{2} \cdot \mathbf{Fs} - \mathbf{Fp}) \cdot \mathbf{Ds}}{\mathbf{2} \cdot \mathbf{Fcg}} \quad \text{(A2)}$$

where:
Fcg: specimen weight
Dcg: specimen CG location (only unknown)
Fp: plate weight
Ds: distance between the support and the scale
Fs: weight measured at the scale

$$\mathbf{I}\ddot{\boldsymbol{\theta}} + \mathbf{K}\boldsymbol{\theta} = \mathbf{0} \quad \text{(A3)}$$

$$\boldsymbol{\omega}_{\mathbf{n}} = \sqrt{\frac{\mathbf{K}}{\mathbf{I}}} = \frac{\mathbf{1}}{\boldsymbol{\tau}_{\mathbf{n}}} \quad \text{(A4)}$$

$$\mathbf{I} = \boldsymbol{\tau}_{\mathbf{n}}^{\,2} \cdot \mathbf{K}$$

where: I: specimen inertia along the torsional spring (only unknown)

K: stiffness of the torsional spring

ωn: natural frequency

τn : measured period from the system

TABLE AI

HEAD AND NECK WEIGHT AND MASS MOMENTS OF INERTIA

UNIT: KG AND KG·CM^2

HD: head, WN: whole neck, UN: upper neck (C1-C4), and LN: lower neck (C4-C7)

	PMHS1	PMHS2	PMHS3	PMHS4	PMHS5	Mean	SD
HD Wt	3.8	3.6	4.3	3.6	3.7	3.8	0.3
HD Ixx	184.8	129.0	164.3	104.3	116.1	139.7	30.2
HD Iyy	200.6	184.3	234.4	182.8	183.6	197.1	19.8
HD Izz	143.9	171.6	208.4	158.3	193.7	175.2	23.3
WN Wt	1.4	1.5	1.6	1.4	1.6	1.5	0.1
WN Ixx	38.6	41.1	46.8	34.8	42.0	40.7	4.0
WN Iyy	33.5	41.7	39.8	31.2	29.2	35.1	4.9
WN Izz	22.4	27.8	30.6	24.4	35.3	28.1	4.6
UN Wt	0.6	0.8	0.8	0.5	0.8	0.7	0.1
UN Ixx	7.2	10.0	13.7	6.9	15.4	10.6	3.4
UN Iyy	6.6	10.7	9.9	5.4	9.2	8.4	2.0
UN Izz	9.8	14.5	17.9	10.2	19.1	14.3	3.8
LN Wt	0.8	0.8	0.8	0.9	0.7	0.8	0.1
LN Ixx	11.7	8.8	12.0	12.4	12.2	11.4	1.3
LN Iyy	9.3	10.7	8.8	10.7	6.7	9.2	1.5
LN Izz	14.0	13.5	15.2	15.0	15.8	14.7	0.8

TABLE AII

MEASURED HEAD CG AND OC LOCATION (RELATIVE TO HEAD AND NECK COORDINATE SYSTEM)

UNIT: CM

HD: head, WN: whole neck, UN: upper neck (C1-C4), and LN: lower neck (C4-C7)

	PMHS1	PMHS2	PMHS3	PMHS4	PMHS5	Mean	SD
HD CGx	-0.75	0.22	-0.16	0.03	0.58	-0.02	0.44
HD CGz	-3.12	-2.72	-3.13	-2.32	-2.78	-2.81	0.30
HD OCx	-1.64	-0.99	-1.52	-1.46	-1.34	-1.39	0.22
HD OCz	2.32	2.54	2.61	3.07	1.63	2.43	0.47
WN CGx	0.55	0.52	1.13	-1.10	-0.67	0.09	0.83
WN CGz	-6.77	-6.29	-6.23	-6.29	-5.95	-6.31	0.26
UN CGx	-0.75	-0.07	1.75	-1.23	-0.49	-0.16	1.03
UN CGz	-9.85	-9.93	-9.09	-10.34	-9.38	-9.72	0.44
LN CGx	0.90	0.75	0.10	-0.81	-1.62	-0.14	0.96
LN CGz	-3.14	-2.88	-3.12	-3.73	-1.84	-2.94	0.62